SF2A 2016
C. Reylé, J. Richard, L. Cambrésy, M. Deleuil, E. Pécontal, L. Tresse and I. Vauglin (eds)

OBSERVATIONS OF FAST RADIO BURSTS AND PERSPECTIVES AT LOW FREQUENCIES

P. Zarka[1] and F. Mottez[2]

Abstract. We briefly summarize the characteristics of the elusive Fast Radio Bursts from existing observations. Then we emphasize the interest of low-frequency observations, e.g. with NenuFAR. In order to define the best observing parameters and detection scheme, we have built a simulation program of FRB at low-frequencies, that proceeds in 2 steps: (i) FRB generation and dilution in a dynamic spectrum with given characteristics, and (ii) definition of the FRB spectrum, and detection on the galactic radio background by means of parametric dedispersion. We carry on a preliminary simulation study, that allows us to draw first conclusions, among which the possibility to detect Lorimer-like FRB with NenuFAR.

Keywords: Fast radio burst, radio astronomy, dynamic spectrum, low frequencies, dedispersion, NenuFAR

1 Introduction

The first Fast Radio Burst (FRB) was discovered in 2007 (Lorimer et al. 2007), and about 20 have been detected since then (Petroff et al. 2016), all but one at ∼1.4 GHz, and one down to 700 MHz (Masui et al. 2015). They consist of a single broadband pulse, of a few milliseconds duration at a given frequency sometimes including an exponentially decreasing tail, and of flux density between 0.1 and 30 Jy at ∼1 GHz. Their main characteristic is that they are dispersed, like pulsar signals but much more dispersed. The signal slides from high to low frequencies with a delay $\delta t(f)$ following very closely the law proportional to DM/f^2 that characterizes radio propagation in a plasma (with DM the dispersion measure, i.e. the integrated electron content along the wave path, in pc.cm^{-3}, and f the frequency of observation). The two main differences between an FRB and pulsar pulses are that (i) an FRB is a unique event (not periodic, although in some cases repetition was observed at variable but generally long intervals (Spitler et al. 2016), and (ii) the dispersion measure DM generally does not exceed ∼100 pc.cm^{-3} for sources out of the galactic plane, whereas the DM of FRB is several hundreds to ≥1000, also for sources out of the galactic plane. After a few years of debate, it is now accepted that FRB are extragalactic signals from sources at hundreds of Mpc to Gpc distances, the large dispersion of which is indeed due to a very large propagation path. As the detected signal is quite intense (0.1−30 Jy), all but one theories proposed for FRB that assume an isotropic emission, require a large energy source $\sim 10^{33}$ J. One theory involves radio beaming in a very narrow angle, of order of 1"[2], and consequently requires a much less energetic emission $\sim 10^{21}$ J (Mottez & Zarka 2014).

Although only ∼20 FRB have been detected until now, the estimated FRB rate is of several thousands/sky/day (e.g. Connor et al. 2016). And basically nothing is known about the FRB spectra, i.e. their spectral slope (Oppermann et al. 2016) or low-frequency cutoff that would provide useful information for constraining their emission mechanism. Observations at GHz frequencies are usually performed in small fields of view ($\ll 1^{\circ 2}$), which explains the low detection rate until now. Al lower frequencies, instruments such as LOFAR (van Haarlem et al. 2013) or NenuFAR (Zarka et al. 2012) have large fields of view, up to $\sim 100^{\circ 2}$. But the FRB signals will be dispersed on much longer times, as the propagation delay varies as f^{-2}. The scattering effect (in $f^{-4.4}$) will also be much stronger. And the galactic background spectrum steeply rises towards low frequencies, as $f^{-2.55}$. It is thus difficult to estimate quantitatively what should be the observations parameters for an optimal low frequency search of FRB, or even if they will be detectable at all.

[1] LESIA & USN, Observatoire de Paris, CNRS, PSL
[2] LUTh, Observatoire de Paris, CNRS, PSL

2 Simulation of low-frequency observations

For that purpose, we have built a simulation program of low-frequency observations aiming at FRB detection. It runs in two steps.

In step 1, we build the dynamic spectrum of a dispersed FRB observed in a selected spectral range [f_{min},f_{max}] with spectral resolution δf and temporal resolution δt. The FRB is defined by its intrinsic fixed frequency duration (excluding any scattering tail) and temporal profile (square, gaussian), its DM, and the e-folding time of its scattering tail if any. The overall duration of the simulated dynamic spectrum must be longer than the dispersion delay from f_{max} to f_{min}, that amounts e.g. to 17870 sec (∼5 hours) through the band [15,85] MHz for DM=1000. The FRB may occur (at f_{max}) at any arbitrary time after the beginning of the dynamic spectrum, but in practice we make it occur before t∼100 sec in order to limit the length (and thus the volume) of the simulated dynamic spectrum. In order to avoid the dilution of the FRB signal in $\delta t \times \delta f$ bins, resolutions better than δt=1 msec and δf=1 kHz should in principle be used. But an observation of 5 hours duration in the [15,85] MHz range with 1 msec×1 kHz duration represents a dynamic spectrum of 1.26 Terapixels. It is thus necessary to observe with coarser resolutions (e.g. δt=10-100 msec and δf=5-25 kHz), with which the large dispersion drift and scattering will indeed cause strong FRB signal dilution. Step 1 of our simulation computes this dilution by using a super-resolved (t, f) grid at 0.1 msec × 0.1 kHz that tracks the burst in the (t, f) plane. The burst shape is computed consecutively for each channel of width δf: the burst is generated undispersed at the above super-resolution with its selected temporal profile and flux density set to 1; then a scattering tail is added (if requested), conserving the total power (or fluence) of the burst, that is the integral of its time profile before scattering; finally, the burst is dispersed with the selected DM, and the dynamic spectrum is rebinned at the chosen $\delta t \times \delta f$. With DM=1000, δt=10-100 msec and δf=25 kHz we find, for an FRB signal of intrinsic fixed-frequency duration 5 msec, a dilution by a factor ∼67 in the resulting dynamic spectrum. The maximum contribution of the FRB, of initial intensity 1 at super-resolution, to a $\delta t \times \delta f$ bin is thus ∼0.015. This dilution, mainly due to the very large dispersion of the signal across the channel width, goes down to a factor ∼13 with δf=5 kHz. An FRB simulated in NenuFAR's range is displayed in Fig. 1.

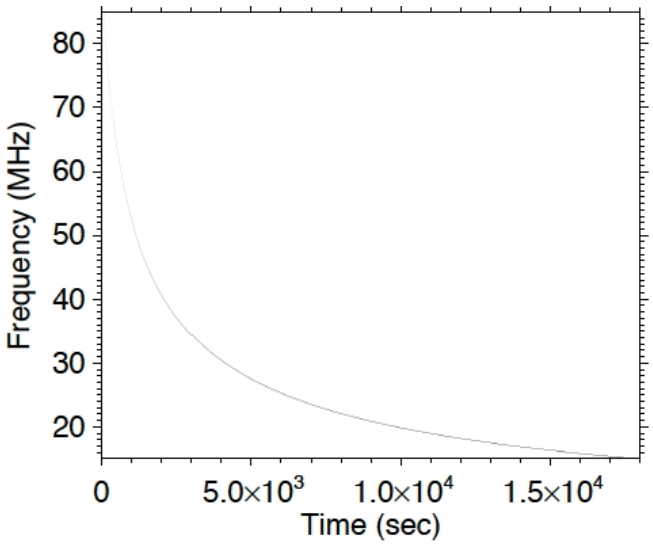

Fig. 1. Simulated FRB in the frequency range of NenuFAR. The burst has a fixed-frequency duration of 5 msec, plus a scattering tail, a DM=1000, and it occurs at $t_\circ$=100 sec at 85 MHz. The dynamic spectrum has resolutions δt=100 msec × δf=25 kHz.

Step 2 starts from the FRB dynamic spectrum generated in step 1. It allows us to define the peak flux density and spectrum of the FRB (flat, power law) that is applied to the dynamic spectrum. Then, the unpolarized sky background is added at each frequency, as an average value plus a random noise representing its statistical fluctuations. The average value at frequency f (i.e. wavelength λ(m)=300/f(MHz)) is: $S_{sky} = 2kT_{sky}/A_{eff}$ with k the Boltzmann constant, T_{sky}(K)=60$\lambda^{2.55}$, and A_{eff} is computed for various user-selected arrays (of dipoles, of LOFAR HBA tiles (van Haarlem et al. 2013), or of NenuFAR mini-arrays (Zarka et al. 2012)). The standard deviation of the random fluctuations is: $\sigma = S_{sky}/(\delta f \times \delta t)^{1/2}$. The FRB hidden in the sky

background fluctuations is then blindly searched for via parametric dedispersion: a ramp of trial DM is tested; for each test DM value, the dynamic spectrum is dedispersed and integrated in frequency to obtain a time series $x(t)$, converted to SNR$(t) = ((x(t) - < x(t) >)/\sigma_x)$, where peaks are then identified. The dynamic spectrum FRB+Sky can be first rebinned to simulate observations with (t, f) resolutions lower than simulated at step 1, and the frequency range of the search can be reduced compared to the range $[f_{min},f_{max}]$ simulated at step 1. Optionally, the dynamic spectrum can be "flattened" (i.e. each spectrum is divided by the average sky background) and smoothed (each fixed-frequency time series is "smoothed" by the dispersive spread within the corresponding channel at the tested DM value) prior to dedispersion.

3 Results

Examples of simulation results are presented in Fig. 2. All panels correspond to an FRB with DM=1000 occurring at $t_\circ$=100 sec (at f_{max}=85 MHz), of duration 5 msec plus a scattering tail of 2 msec at 85 MHz (increasing as $f^{-4.4}$ at lower frequencies), observed with resolutions δt=100 msec (rows #1 to #4) or 10 msec (rows #5 and #6) and δf=25 kHz, in the range 15−85 MHz with the NenuFAR array (at completion, with 96 arrays of 19 dipoles (Zarka et al. 2012)). Row #1 (top) corresponds to an FRB with a flat spectrum of flux density S=1000 Jy. It is easily detected in the 15−85 MHz range, applying flattening and smoothing, with SNR>80. Row #2 corresponds to similar results for S=100 Jy: here the SNR is only ∼7. Note that in both cases DM and $t_\circ$ are biased toward slightly larger values than those used at step 1, due to the scattering tail. Rows #3 and #4 are similar to row #2 except that no smoothing is applied. The strongest peak is obtained at a time different from $t_\circ$ and DM=990 (row #3). A peak with lower SNR is found at $\sim t_\circ$ and DM∼1000 (row #4). However, it can be noticed that the shape of the peak in the (DM,t) plane (panel 4a) as well as in the time series SNR(t) (panel 4b) in row #4 is similar to those in rows #1 and #2, which is not the case for the spurious peak of row #3. Thus discrimination of real signal peaks should be possible. But this also shows that smoothing improves detectability. With a flat spectrum at S=30 Jy, the FRB is no more detected in the range 15−85 MHz with NenuFAR. Row #5 shows the results obtained with a similar simulation but with δt=10 msec, for an FRB with a spectrum S(Jy)=30×$(f/85\ \text{MHz})^{-0.7}$, searched for in the 32−85 MHz range. As in row #3 the main peak is not the FRB at $t_\circ$=100 sec and DM=1000, but a spurious peak at another time (panel 5b) and DM=1006 (panels 5a and 5c), but one of the few detected peaks with highest SNR is indeed the simulated FRB (row #6).

4 Conclusions

This is a preliminary simulation study, as the parameter space to explore is vast. But the developed tools have been tested and validated. This study shows that:

- a good spectral resolution, better than a few kHz, is important for reducing the FRB signal dilution ;
- a time resolution of ∼10 msec/spectrum is acceptable for an FRB search ;
- smoothing (by the dispersive spread in each spectral channel) improves SNR and thus detectability ;
- an FRB with flux density ∼30 Jy and fixed-frequency duration 5 msec (similar to the Lorimer burst (Lorimer et al. 2007), but with DM up to 1000), can be detected with NenuFAR ; note that although this flux density corresponds to the strongest FRB detected at ∼1.4 GHz, it is a modest flux density at the much lower frequency studied here as the spectrum may rise toward low frequencies ;
- analysis of the shape of the detected peaks in the (DM,t) plane and in a time series SNR(t) should allow us to discriminate between genuine FRB and spurious peaks.

The present analysis assumes no effect from RFI (interference) nor ionospheric fluctuations. The latter should not strongly influence detectability, and the residual effect of the former (that should be mitigated prior to dedispersion) will be much reduced by the dedispersion with a large DM. We conclude that FRB search will be worth to carry on at low frequencies, e.g. with NenuFAR. If detection occurs, it will bring important information about FRB occurrence, distribution in the sky, spectrum, low-frequency cutoff, and polarization. The developed simulation program may be used for optimizing the observations of FRB, RRAT (Rotating RAdio Transients (McLaughlin et al. 2006)), or pulsar single pulses with various low-frequency instruments.

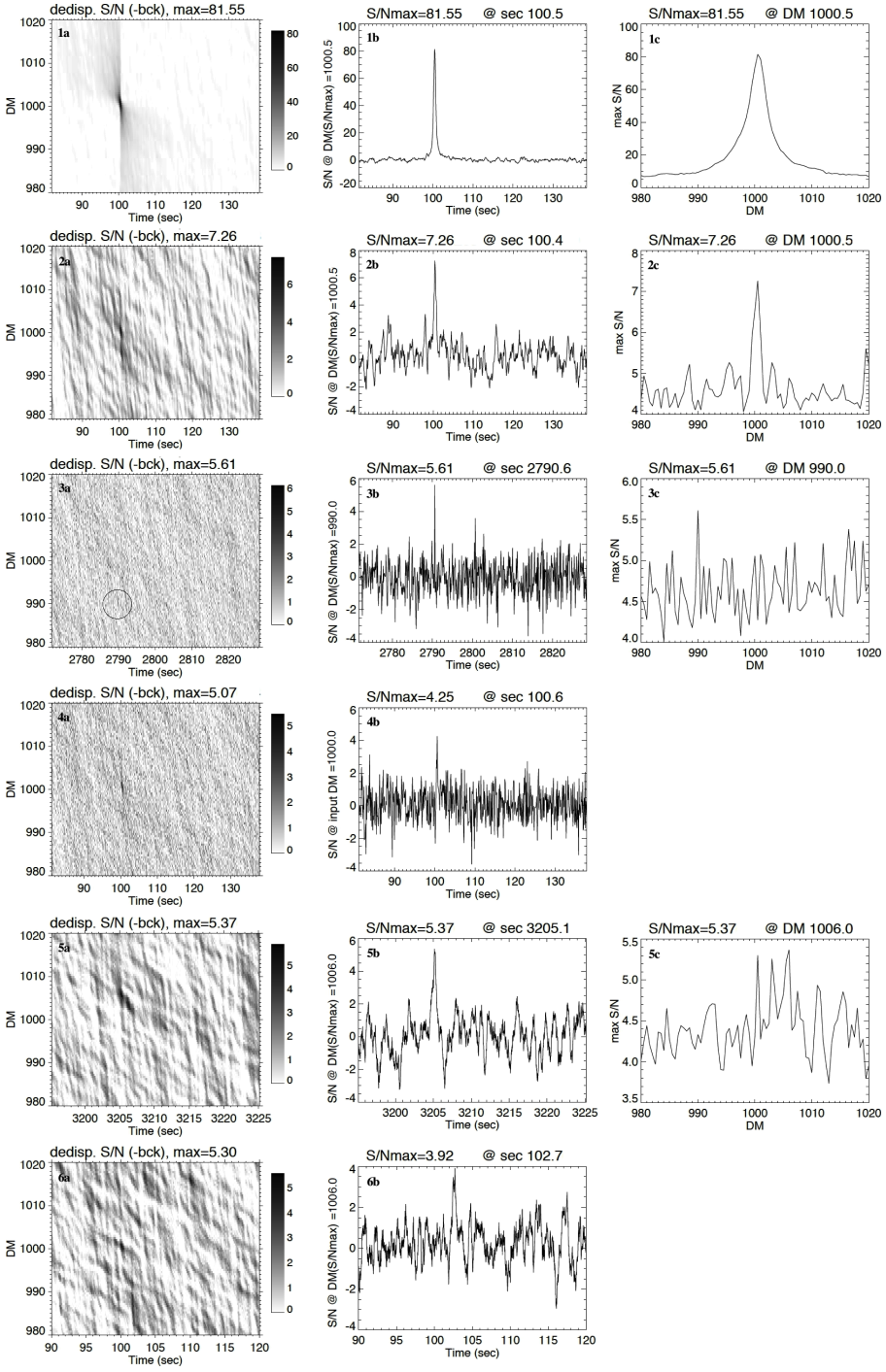

Fig. 2. Simulation tests of detection of the FRB of Fig. 1. Row #1: the FRB has a flat spectrum of 1000 Jy. Row #2: the FRB has a flat spectrum of 100 Jy. Rows #3 and #4: same as row #2 but no smoothing applied in the detection scheme. Rows #5 and #6: the dynamic spectrum (of Fig. 1) has a time resolution δt=10 msec and is restricted to the 32−85 MHz range. The FRB has a flux density spectrum of $30\times(f/85\ \mathrm{MHz})^{-0.7}$. Column *a*: dedispersed and integrated time series as a function of the DM (on panel 3a, the peak SNR value is an isolated pixel near the center of the circle). Column *b*: time profile obtained by dedispersion with the DM indicated on the y-axis and spectral integration, around the time of maximum SNR (rows #1,2,3,5) as well as around $t_\circ$ (rows #1,2,4,6). Column *c*: maximum SNR of the time series obtained for each DM. See text (section 3) for details.

References

Connor, L., Lin, H.-H., Masui, K., et al. 2016, MNRAS, 460, 1054

Lorimer, D. R., Bailes, M., McLaughlin, M. A., Narkevic, D. J., & Crawford, F. 2007, Science, 318, 777

Masui, K., Lin, H.-H., Sievers, J., et al. 2015, Nature, 528, 523

McLaughlin, M. A., Lyne, A. G., Lorimer, D. R., et al. 2006, Nature, 439, 817

Mottez, F. & Zarka, P. 2014, A&A, 569, A86

Oppermann, N., Connor, L. D., & Pen, U.-L. 2016, MNRAS, 461, 984

Petroff, E., Barr, E. D., Jameson, A., et al. 2016, PASA, 33, e045

Spitler, L. G., Scholz, P., Hessels, J. W. T., et al. 2016, Nature, 531, 202

van Haarlem, M. P., Wise, M. W., Gunst, A. W., et al. 2013, A&A, 556, A2

Zarka, P., Girard, J. N., Tagger, M., & Denis, L. 2012, in SF2A-2012: Proceedings of the Annual meeting of the French Society of Astronomy and Astrophysics, ed. S. Boissier, P. de Laverny, N. Nardetto, R. Samadi, D. Valls-Gabaud, & H. Wozniak, 687–694